ACS APPLIED MATERIALS & INTERFACES

Research Article

www.acsami.org

Selective Inactivation of Resistant Gram-Positive Pathogens with a Light-Driven Hybrid Nanomaterial

Malte Grüner,[†] Lorena Tuchscherr,[§] Bettina Löffler,[§] Dominik Gonnissen,[†] Kristina Riehemann,[†] Mark C. Staniford,[‡] Ulrich Kynast,[‡] and Cristian A. Strassert*[,†]

[†]Westfälische Wilhelms-Universität Münster, Physikalisches Institut - Center for Nanotechnology, Heisenbergstrasse 11, 48149 Münster, Germany

[‡]Münster University of Applied Sciences, Institute for Optical Technologies, Stegerwaldsstrasse 39, 48565 Steinfurt, Germany

[§]Universitätsklinikum Jena, Institut für Medizinische Mikrobiologie, Erlanger Allee 101, 07747 Jena, Germany

Supporting Information

ABSTRACT: Herein, we present a straightforward strategy to disperse highly insoluble photosensitizers in aqueous environments, without major synthetic efforts and keeping their photosensitizing abilities unaffected. A layered nanoclay was employed to adsorb and to solubilize a highly efficient yet hydrophobic Si(IV) phthalocyaninate in water. The aggregation of the photoactive dye was correlated with its photophysical properties, particularly with the ability to produce highly cytotoxic singlet oxygen. Moreover, the resulting hybrid nanomaterial is able to selectively photoinactivate Gram-positive pathogens, due to local interactions between the bacterial membranes and the negatively charged nanodiscs. Nanotoxicity assays confirmed its innocuousness toward eukaryotic cells, showing that it constitutes a new class of "phototriggered magic bullet" for the inactivation of pathogens in phototherapy, as well as in the development of coatings for self-disinfecting surfaces.

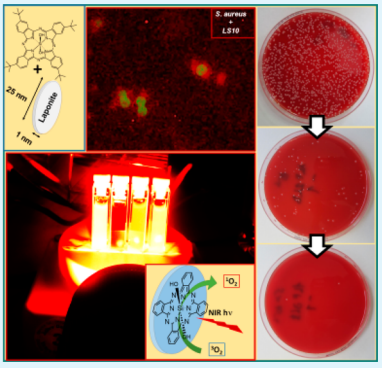

KEYWORDS: *nanomaterial, nanoclay, photosensitizer, singlet oxygen, phthalocyanine, antibiotic resistant bacteria, photodynamic inactivation, phototherapy*

INTRODUCTION

Bacterial resistance against antibiotics and difficult-to-treat infections are considered among the major challenges in public health and modern pharmacology.[1−4] In the United States and Europe alone, around 50 000 deaths annually can be related to this problem, causing immense costs for the health system.[5,6] Phototherapy is commonly used in the treatment of cancer and macular degeneration, but the same principles can be applied for inactivation of antibiotic-resistant or antibiotic-tolerant infections.[7−9] Briefly, irradiation with visible light causes the production of cytotoxic $^1O_2$ by collisional energy transfer from a photosensitizing dye to $^3O_2$ in solution or at a surface.[10,11] Phthalocyanines are particularly suited for the development of phototherapeutic agents due to their efficient $^1O_2$ generation, intense red-light absorption, low toxicity, and high stability.[12−14] In order to retain the photosensitizing characteristics of these macrocycles, aggregation must be avoided.[15,16] One strategy involves the axial functionalization of Si(IV) phthalocyanines, which has been successfully applied in the treatment of cancer leading to the FDA-approved phototherapeutic drug Pc4.[17,18] The prevention of prevalent infections also includes the development of self-cleaning surfaces, as well as the affordable supply of drinking water. Several approaches have been explored, including the use of silver nanoparticles in self-cleaning surfaces and of chemical, electrochemical, or photochemical methods for the decontamination of drinking water.[19−25]

The use of nanomaterials as targeted therapeutic, sensing, and imaging agents relies on surface modification with suitable bioactive functionalities.[26−29] In a previous article, we have shown that photoactive nanomaterials can be suitably designed employing Si(IV) phthalocyanines axially bound onto zeolite L nanocrystals, where the resulting hybrid nanomaterial was able to target, to label, and to photoinactivate antibiotic-resistant Gram-negative pathogens such as *E. coli* and *N. gonorrheae*.[30,31] The surface functionalization and charge can be directly correlated with the photophysical properties, showing that the dispersibility in water as well as the interaction with Gram-negative bacteria is favored by positive surface charges.[32] However, zeolite L crystals do not provide fully transparent dispersions, and the aqueous suspensions tend to show limited stabilities.[33] Furthermore, Gram-positive bacteria need to be addressed as well, due to their clinical relevance. On the other hand, Laponite RD is a nontoxic nanoclay consisting of disc-shaped nanoparticles forming stable dispersions in water. This interesting nanomaterial has found applications in the formulation of water-based coatings, as it facilitates the

Received: July 24, 2015
Accepted: August 25, 2015
Published: August 25, 2015

DOI: 10.1021/acsami.5b06742
ACS Appl. Mater. Interfaces 2015, 7, 20965−20971

solubilization of pigments in aqueous environments. In particular, we have recently demonstrated that Laponite can be used to disperse highly hydrophobic pigments such as indigo blue in water, and the correlation between the aggregation of the dye and its optical properties was investigated.[34,35] Besides its applications in materials science, its lack of toxicity also renders it an interesting additive for pharmaceutical, cosmetic, and food formulations.[36−40] Moreover, its application as a drug carrier has been proposed,[41,42] for instance, to enhance the selective uptake and accumulation of the chemotherapeutic drug doxorubicin by neoplastic cells.[43−45] Herein, we present a hybrid nanomaterial that can be easily obtained by adsorbing axially and peripherally substituted Si(IV) phthalocyanines onto Laponite, yielding stable and transparent aqueous dispersions. The photophysical properties can be precisely correlated with the aggregation of the photosensitizer, and the interactions between the negatively charged discs and the bacterial surfaces enable the selective photoinactivation of Gram-positive bacteria in the presence of Gram-negative species by irradiation with red light. Suitable nanotoxicity assays corroborated the lack of toxicity toward eukaryotic cells.

RESULTS AND DISCUSSION

Synthesis. Laponite nanodiscs, 25 nm in diameter and 1 nm in thickness, were loaded with tetra-*tert*-butyl-substituted Si^{IV} phthalocyanine dihydroxide (SiPc) as a photosensitizer (PS) (Scheme 1). Due to the peripheral *t*-butyl groups, aggregation is hindered, whereas the OH groups favor axial binding onto the surface of the nanodiscs. The PS was dissolved in toluene and readily adsorbed onto the surface of the nanodiscs by overnight stirring, followed by repeated suspension in fresh toluene and centrifugation. Three different loading ratios were investigated, namely, 1, 10, and 100 mg of SiPc/g of Laponite, yielding three different nanomaterials (**LS1**, **LS10**, and **LS100**, respectively, Scheme 1). Spectrophotometric quantification of the PS in the mother liquors pointed toward a quantitative adsorption for **LS1** and **LS10** (no traceable dye in the supernatants). For **LS100**, however, the surface appears saturated, as part of the PS is washed off. The actual loadings are listed in Table 1, taking into account the initial amount of PS and the desorbed dye (see also Supporting Information for further details). Interestingly, the ζ-potential rises (less negative) with increasing loadings, as well as the particle size measured by DLS. This indicates that the SiPc at the surface leads to a higher hydrophobicity, which causes the formation of clusters of nanodiscs with increasing size.

Scheme 1. Synthetic Route Towards Laponite Nanodiscs with Three Different Loadings: LS1, LS10, and LS100[a]

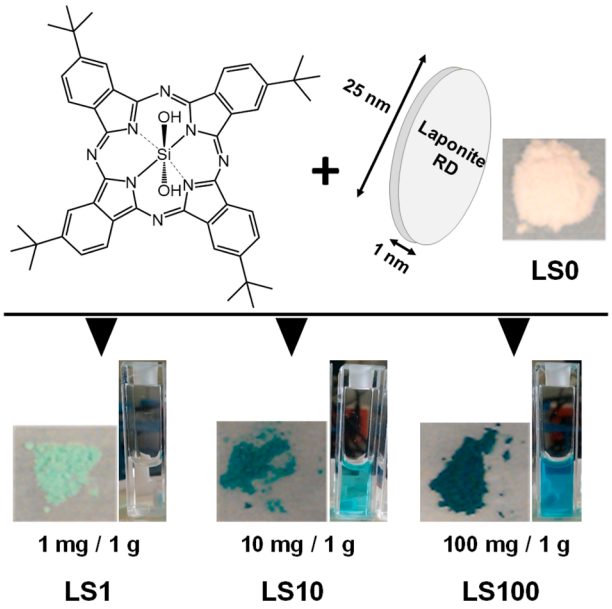

[a]The solid materials and the dispersions (2 mg/mL) in distilled water are depicted.

Table 1. Size Determined by Dynamic Light Scattering (DLS), ζ-Potential, and Loading with SiPc of LS0, LS1, LS10, and LS100

sample	size (nm)	ζ-potential (mV)	loading (mmoles SiPc/ 1 g Laponite)
LS0	33.6	−45.8	0
LS1	36.3	−34.4	0.00125
LS10	62.7	−26.3	0.0125
LS100	92.4	−21.6	0.123

Photophysics. The photophysical properties of the hybrid nanodiscs are summarized in Table 2, including the absorption, excitation, and emission maxima, the fluorescence (Φ_F) and singlet oxygen (Φ_Δ) quantum yields, and the fluorescence lifetimes (τ_F) (the corresponding spectra and decays can be found in Figures S2−S8). For comparison, dilute solutions of SiPc in DCM provided the quantum yields of the monomeric species of the phthalocyaninate, namely, Φ_F = 0.52 and Φ_Δ = 0.47 (τ_F = 5.34 ns).[33] When the loading is increased, the progressive formation of aggregates at the surfaces can be traced by monitoring the growth of a blue-shifted shoulder on the Q-band (H-type),[46] as well as of a red-shifted band above 750 nm (J-type)[47] (Figure 1), which are both characteristic for phthalocyaninates. This trend is also reflected in the quantum yields, Φ_F drops from 14% to 5% and 1%, whereas Φ_Δ decreases from 14% to 8% and 5% for **LS1**, **LS10**, and **LS100**, respectively (Table 2).

Homo-FRET is most likely responsible for the observed drops, by funneling the excitons along the nanodiscs toward energy traps (inactive aggregates) that ultimately lead to thermal dissipation.[48] Therefore, closer lateral dye distances also cause a progressive shortening of the excited state lifetimes (Table 2), whereas the shape of the fluorescence spectra remains unaffected when going from **LS1** to **LS100** (Figure S2). The latter observation points toward a negligible self-absorption (i.e., trivial energy transfer) for dilute dispersions of the nanodiscs. However, when the concentration of nanoparticles in water is increased for a given load, trivial energy transfer between the particles is switched on: the τ_F lengthens, Φ_F drops (Tables S1 and S2), and the relative intensity of the red-shifted vibrational shoulder of the fluorescence spectrum is enhanced (Figure S3). Besides this optical density-related effect, interparticle aggregation does not significantly affect the photophysical properties of the nanodiscs (Figures 1 and S7 and Table S2). Interestingly, high concentrations of nanodiscs lead to weakly fluorescent hydrogels, which become photoactive upon dilution and monomerization of the nanodiscs.

Photoinactivation. In order to investigate the photobactericidal potential, suspensions of *S. aureus* 6850 (Table S3), a Gram-positive pathogen, were treated with dispersions of the

DOI: 10.1021/acsami.5b06742
ACS Appl. Mater. Interfaces 2015, 7, 20965−20971

Table 2. Photophysical Properties of LS1, LS10, and LS100

sample	Φ_F (±0.02)	Φ_Δ (±0.05)	λ_{abs}/nm	λ_{em}/nm	τ/ns
LS1	0.14	0.14	622; 658; 692	697	4.31 (100%)
LS10	0.05	0.08	624; 649; 690	699	4.15 (95%); 0.83 (5%)
LS100	0.01	0.05	630; 647; 692	699	3.79 (84%); 0.81 (16%)

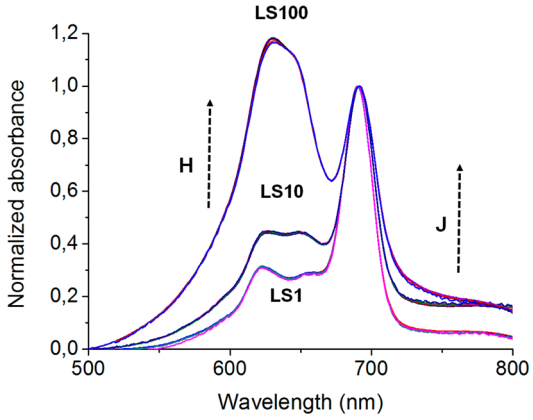

Figure 1. Normalized absorption spectra of **LS1**, **LS10**, and **LS100** in water at room temperature for five different concentrations of loaded Laponite ranging from 0.0008 to 8 mg/mL.

nanodiscs (2 mg/mL) and irradiated with a weak polychromatic light source (10.0 mW/cm^2) with a cutoff filter at 610 nm for up to 4 h (total radiant exposure: 144 J/cm^2). Thus, the photosensitizer is selectively excited and produces cytotoxic $^1O_2$. Aliquots of samples and controls were taken in 60 min intervals, and several dilutions (up to 10^{-7} of the original bacterial concentration) were plated on Petri dishes with sheep-blood feeding grounds (Figure S9). A statistical analysis of the number of colony forming units (CFUs) after 20 h of incubation delivered the number of remaining bacteria in the irradiated samples (dark and **LS0**, i.e., native Laponite, were also analyzed, for comparison). **LS1** particles did not show any effect on the number of CFUs, whereas **LS10** and **LS100** significantly reduced the amount of bacteria (Figure S10). Notably, **LS10** and **LS100** inactivated 99.9% and 80% of the bacteria, respectively. Although the **LS1** particles have the best quantum yields, it is clear that the concentration of SiPc is too low, as well as the resulting amount of $^1O_2$. The most efficient inactivation is reached with **LS10** particles, where the amount of $^1O_2$ is sufficient and aggregation phenomena do not compromise the performance to a large extent (*vide supra*). Higher loadings with SiPc do not correlate with further inactivation enhancements, despite the fact that, in principle, more PS molecules are available. Aggregation and homo-FRET between adjacent molecules most likely compete with energy transfer to molecular oxygen, which would ultimately lead to $^1O_2$.

Comparable photoinactivation experiments with Gram-negative pathogenic bacteria, such as *E. coli* and *E. cloacae*, indicated that only Gram-positive species (such as the pathogens *S. aureus* 6850, *S. aureus* USA300 (MRSA), *S. aureus* Cowan I, and *E. faecalis*) are significantly affected by the photoactive nanodiscs (for further details, see Figures S11 and S12 and Table S3). **LS10** was further used to treat a mixture of *S. aureus 6850* and *E. coli*, in order to evaluate the selective recognition and phototoxicity when both types of bacteria are present at similar concentrations. After irradiation, the growth on Petri dishes with different feeding grounds such as sheep-blood agar (nonselective), SAID agar (selective for *S. aureus*), and MacConkey agar (selective for *E. coli*) permitted the evaluation of the number of CFUs of every type of bacteria. In Figure 2, the bacterial count is represented as a function of the

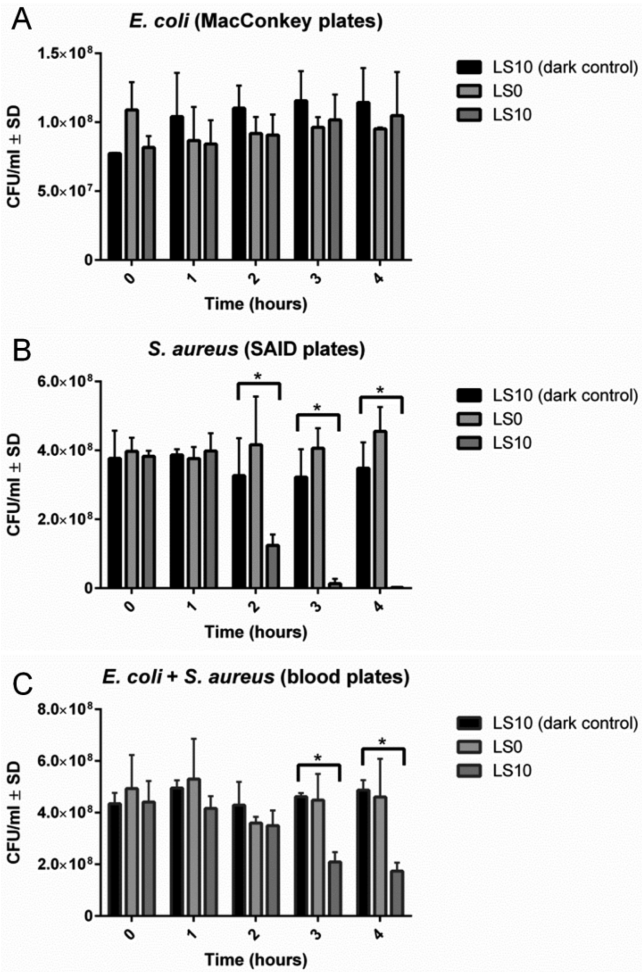

Figure 2. Number of colony forming units (CFUs) of *E. coli* and *S. aureus* 6850 treated with **LS10** and irradiated. The number of CFUs was determined using (A) *E. coli*-selective plates (MacConkey), (B) *S. aureus* selective plates (SAID), and (C) plates on which both bacteria can grow (sheep-blood).

light dose. It is clear that, even in the mixture, *E. coli* bacteria remain unaffected by the irradiation (MacConkey plates), whereas SAID dishes show that 99.9% of the *S. aureus* bacteria are inactivated (Figure S13). The ability of the nanodiscs to discriminate between different classes of bacteria was further investigated by fluorescence and scanning electron microscopies (SEM). Upon addition of **LS10** to a suspension of fluorescein-stained *E. coli*, no colocalization of the red-fluorescent nanodiscs and the green bacteria was detected, as opposed to the distinct correlation between the red fluorescence of the nanodiscs and the green-fluorescence-

DOI: 10.1021/acsami.5b06742
ACS Appl. Mater. Interfaces 2015, 7, 20965−20971

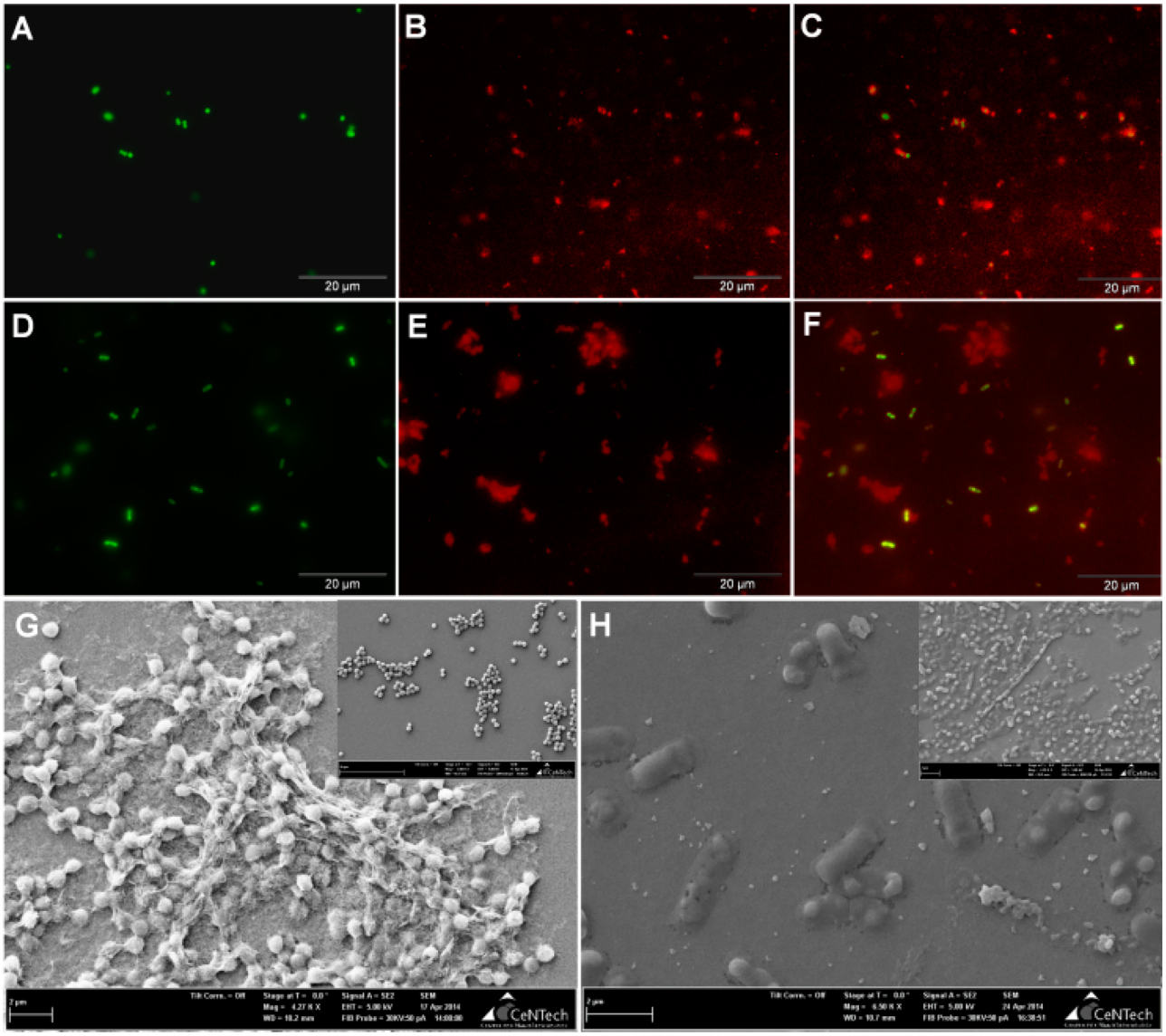

Figure 3. Fluorescence micrographs of *S. aureus* 6850 (A), **LS10** (B), and the merged image (C). Fluorescence micrographs of *E. coli* (D), **LS10** (E), and the merged image (F). SEM images of **LS10** with *S. aureus* 6850 (G) and with *E. coli* (H), the insets represent bacterial samples without nanodiscs.

labeled *S. aureus* 6850 bacteria (Figures 3, S14, and S15). The scanning electron micrographs confirmed these findings: *S. aureus* 6850 bacteria appear entrapped in a network of **LS10** as a carpet of filaments, whereas *E. coli* and **LS10** do not show any significant colocalization (Figures 3 and S16). The selectivity can be attributed to local interactions of the nanodiscs and the peptidoglycan layer of Gram-positive bacteria, whereas the outer membrane of Gram-negative species hinders such interactions. The resulting distance between the biological target and the PS that photoproduces $^1O_2$ is too large for Gram-negative bacteria in relation to the diffusion range of $^1O_2$ (268 nm).[49]

CONCLUSION

As Laponite is already employed in cosmetic formulations, our nanomaterial could be implemented for the phototherapy of infections, particularly on skin-related conditions. Indeed, nanotoxicity assays with primary dermal fibroblast cells and a COLO-818 cell line indicate that, both with and without red-light irradiation, no damage is inflicted by **LS10** toward eukaryotic cells (Figure S17). Thus, a hydrogel of the nanomaterial could be used to treat the affected area and subsequently selectively irradiated. Only the regions where the monomeric discs are available (for instance, at the bacterial surface) would be exposed to $^1O_2$ upon directed irradiation with harmless red light, which is able to deeply penetrate into tissues. Moreover, the development of self-disinfecting surface coatings can be envisaged. Actually, Laponite is currently used as a thixotropic agent in numerous formulations of water-based lacquers, and a tailored combination of phthalocyanine-loaded nanodiscs with bacteriostatic cations added by ion exchange (e.g., with benzalchonium chloride) lies at hand, as well as the use of other photosensitizers. The combination of bacteriostatic and phototoxic properties, which could also extend the activity against Gram-negative species, is the object of ongoing research in our laboratories.

DOI: 10.1021/acsami.5b06742
ACS Appl. Mater. Interfaces 2015, 7, 20965−20971

EXPERIMENTAL SECTION

Chemicals. Silicon 2,9,16,23-tetra-*tert*-butyl-29*H*,31*H*-phtalocyanine dihydroxide (SiPc, M_w: 799.06 g/mol) was purchased from Sigma-Aldrich. The solvents (Merck) were analytical grade and used without further purification. The Laponite RD nanomaterial was purchased from Rockwood Additives and used without modification and is further referred to simply as Laponite.

Dynamic Light Scattering Measurements. Dynamic light scattering (DLS) and ζ-potential measurements were carried out in bidistilled water with a Malvern Instrument (Zetasizer, Nano ZS).

Instrumentation for Spectroscopy. Absorption spectra were measured on a Varian Cary 5000 double-beam UV−vis-NIR spectrometer and baseline corrected. Steady-state emission spectra were recorded on a FluoTime300 spectrometer from PicoQuant equipped with a 300 W ozone-free Xe lamp (250−900 nm), a 10 W Xe flash-lamp (250−900 nm, pulse width <10 μs) with repetition rates of 0.1−300 Hz, an excitation monochromator (Czerny-Turner 2.7 nm/mm dispersion, 1200 grooves/mm, blazed at 300 nm), diode lasers (pulse width <80 ps) operated by a computer-controlled laser driver PDL-820 (repetition rate up to 80 MHz, burst mode for slow and weak decays), two emission monochromators (Czerny-Turner, selectable gratings blazed at 500 nm with 2.7 nm/mm dispersion and 1200 grooves/mm or blazed at 1250 nm with 5.4 nm/mm dispersion and 600 grooves/mm), Glan-Thompson polarizers for excitation (Xe-lamps) and emission, a Peltier-thermostatized sample holder from Quantum Northwest (−40 to 105 °C), and two detectors, namely, a PMA Hybrid 40 (transit time spread fwhm <120 ps, 300−720 nm) and a R5509-42 NIR-photomultiplier tube (transit time spread fwhm 1.5 ns, 300−1400 nm) with external cooling (−80 °C) from Hamamatsu. Steady-state and fluorescence lifetimes were recorded in TCSPC mode by a PicoHarp 300 (minimum base resolution 4 ps). Emission and excitation spectra were corrected for source intensity (lamp and grating) by standard correction curves. Lifetime analysis was performed using the commercial FluoFit software. The quality of the fit was assessed by minimizing the reduced chi squared function (χ^2) and visual inspection of the weighted residuals and their autocorrelation. Luminescence quantum yields were measured with a Hamamatsu Photonics absolute PL quantum yield measurement system (C9920-02) equipped with a L9799-01 CW Xenon light source (150 W), monochromator, C7473 photonic multichannel analyzer, and integrating sphere and employing U6039-05 PLQY measurement software (Hamamatsu Photonics, Ltd., Shizuoka, Japan). All solvents used were of spectrometric grade.

Singlet Oxygen Quantum Yields. The singlet oxygen quantum yields of **LS1**, **LS10**, and **LS100** (Φ_Δ) were measured in water in order to address their use in aqueous media. Due to the low phosphorescence intensity of the spin-forbidden radiative $^1O_2 \rightarrow {}^3O_2$ transition, $^1O_2$ photogeneration rates were derived using 9,10-anthracenediyl-bis(methylene)dimalonic acid (ABMDMA) as a fluorescent monitor (λ_{ex} = 380 nm) for photosensitized bleaching rates. Polychromatic irradiation from a projector lamp (Leica ZETT Royal II afs) passing through a cutoff filter at 610 nm was used to carry out the experiments (Figure S8 and further details are described in the Supporting Information).

Photoinactivation of Bacteria. One mL of Laponite dispersion (see Supporting Information for further details) was filled into a quartz cuvette (10 mm × 10 mm), and 1 mL of bacterial suspension was added. The irradiation was realized with polychromatic light of a projector lamp passing through a 610 nm cutoff filter (10 mW/cm^2) for a time lapse of 4 h (total radiant exposure: 144 J/cm^2), while the temperature remained constant within 5 °C of room temperature (22 °C). Mixing occurred throughout the experiment by magnetic stirring bars. Aliquots of 10 μL were taken out of the cuvettes after defined time intervals (every 60 min) and diluted further until a dilution factor of 10^{-7} of the original concentration of the bacterial suspension was reached. The dilutions were plated out on Petri-dishes with either sheep-blood as feeding grounds, *S. aureus*-selective SAID plates, or *E. coli*-selective MacConkey plates. Colony forming units (CFUs) were counted 18 h after incubation of the plates. The relationship between all the data was established by the one way ANOVA test with the Dunnett's multicomparison post-test (**LS10** dark control in comparison with **LS0** and **LS10**). Significance was calculated using the GraphPad Prism 6.0 software. To monitor the irradiation effect of the different loadings, **LS0**, **LS1**, **LS10**, and **LS100** particles were directly compared within the course of an irradiation experiment employing *S. aureus 6850* bacteria.

Fluorescence Staining of Bacteria. Five mg of fluorescein 5(6)-isothiocyanate (FITC) on Celite (10%) were suspended in 5 mL of Na_2CO_3 buffer solution and centrifuged at 13 000*g* for 10 min. The bacteria were prepared as mentioned in the Supporting Information, and the suspension was centrifuged to form a bacterial pellet, which was resuspended in 2 mL of FITC solution and incubated for 30 min in the dark. The resulting suspension was centrifuged (4000 rpm, 8 min), and the remaining bacterial pellet was washed twice with PBS. The OD_{600} was set to 1, and the Laponite dispersion was added to obtain a volumetric ratio of 1:1.

Fluorescence Microscopy. Fluorescence microscopy images were recorded on an Olympus IX71 microscope equipped with a XC10 color CCD camera and a xenon lamp as excitation source. FITC was selectively excited with light passing through a 470−490 nm band-pass filter, and emission was recorded through a 400 nm dichroic filter and a 420 nm long-pass filter. SiPc on Laponite was selectively excited with light passing through a 620−660 nm band-pass filter, and emission was recorded through a 670 nm dichroic filter and a 660−720 nm band-pass filter.

Scanning Electron Microscopy. The samples were deposited onto silicon dioxide substrates via drop casting. After drying of the samples, they were covered by a 5 nm thick silver layer via sputtering. The samples were finally investigated using a Zeiss 1540 EsB dual beam focused ion beam/field emission scanning electron microscope, with a working distance of 8 mm and an extra high tension (EHT) of 3 kV.

Cytotoxicity Assays. The primary dermal fibroblast cells (ATCC, USA) were cultured in fibroblast basal medium supplemented with fibroblast growth kit low serum (ATCC, USA). The COLO-818 cell line (DSMZ, Germany) was cultivated in RPMI 1640 containing 10% fetal bovine serum (Biochrom, Germany). Both cell lines were incubated at 37 °C and 5% CO_2 in a humidified atmosphere. For the cytotoxicity assays (Promega, USA), 3.6×10^3 cells were seeded in 96-well plates and, after a 12 h preincubation, incubated for 24 h with different nanoparticle concentrations. After 24 h of incubation, the plates were kept in the dark or irradiated at 600 nm with 530 μW for 4 h (7.6 J/cm^2). Luminescence was measured using a FluoStar Optima microplate reader. For evaluation, toxicity was determined as the fold increase of the negative control.

ASSOCIATED CONTENT

Supporting Information

The Supporting Information is available free of charge on the ACS Publications website at DOI: 10.1021/acsami.5b06742.

Detailed information regarding the loading process and its quantification, the Laponite dispersion procedure, the bacterial suspension procedure, steady-state and time-resolved spectroscopy data, further photoinactivation results, additional fluorescence microscopy and SEM images, and the results of the cytotoxicity assays (PDF)

AUTHOR INFORMATION

Corresponding Author

*E-mail: ca.s@wwu.de.

Notes

The authors declare no competing financial interest.

DOI: 10.1021/acsami.5b06742
ACS Appl. Mater. Interfaces 2015, 7, 20965−20971

■ ACKNOWLEDGMENTS

Financial support from the Deutsche Forschungsgemeinschaft (DFG, Project STR1186/1-1) is gratefully acknowledged.

■ REFERENCES

(1) WHO. *The Evolving Threat of Antimicrobial Resistance- Options for Action*; World Health Organization: Geneva, Switzerland, 2012.
(2) Fair, R. J.; Tor, Y. Antibiotics and Bacterial Resistance in the 21st Century. *Perspect. Med. Chem.* **2014**, *6* (1), 25−64.
(3) Ellington, M. J.; Reuter, S.; Harris, S. R.; Holden, M. T.; Cartwright, E. J.; Greaves, D.; Gerver, S. M.; Hope, R.; Brown, N. M.; Török, M. E.; Parkhill, J.; Köser, C. U.; Peacock, S. J. Emerging and Evolving Antimicrobial Resistance Cassettes in Community-Associated Fusidic Acid and Methicillin-Resistant *Staphylococcus aureus*. *Int. J. Antimicrob. Agents* **2015**, *45* (5), 477−484.
(4) Pogue, J. M.; Kaye, K. S.; Cohen, D. A.; Marchaim, D. Appropiate Antimicrobial Therapy in the Era of Multidrug-Resistant Human Pathogens. *Clin. Microbiol. Infect.* **2015**, *21* (4), 302−312.
(5) Centers for Disease Control and Prevention (CDC). *Antibiotic Resistance Threats in the United States, 2013*; CDC: Atlanta, 2013.
(6) Ridge, K. W.; Hand, K.; Sharland, M.; Abubakar, I.; Livermore, D. M. *Annual Report of the Chief Medical Officer, 2011*; Department of Health: London, 2013; Vol. 2; Chapter 5.
(7) Scalise, I.; Durantini, E. N. Synthesis, Properties, and Photodynamic Inactivation of Escherichia coli Using a Cationic and a Noncharged Zn(II) Pyridyloxyphthalocyanine Derivatives. *Bioorg. Med. Chem.* **2005**, *13* (8), 3037−3045.
(8) Huang, L.; Dai, T.; Hamblin, M. R. Antimicrobial Photodynamic Inactivation and Photodynamic Therapy for Infections. *Methods Mol. Biol.* **2010**, *635*, 155−173.
(9) Sperandio, F. F.; Huang, Y.-Y.; Hamblin, M. R. Antimicrobial Photodynamic Therapy to Kill Gram-negative Bacteria. *Recent Pat. Anti-Infect. Drug Discovery* **2013**, *8* (2), 108−120.
(10) Mirenda, M.; Strassert, C. A.; Dicelio, L. E.; San Román, E. Dye-Polyelectrolyte Layer-by-Layer Self-Assembled Materials: Molecular Aggregation, Structural Stability, and Singlet Oxygen Photogeneration. *ACS Appl. Mater. Interfaces* **2010**, *2* (6), 1556−1560.
(11) Schweitzer, C.; Schmidt, R. Physical Mechanisms of Generation and Deactivation of Singlet Oxygen. *Chem. Rev.* **2003**, *103* (5), 1685−1757.
(12) Regehly, M.; Greish, K.; Rancan, F.; Maeda, H.; Böhm, F.; Röder, B. Water-Soluble Polymer Conjugates of ZnPP for Photodynamic Tumor Therapy. *Bioconjugate Chem.* **2007**, *18* (2), 494−499.
(13) Ishii, K. K.; Shiine, M.; Shimizu, Y.; Hoshino, S.; Abe, H.; Sogawa, K.; Kobayashi, N. Control of Photobleaching in Photodynamic Therapy Using the Photodecarbonylation Reaction of Ruthenium Phthalocyanine Complexes via Stepwise Two-Photon Excitation. *J. Phys. Chem. B* **2008**, *112* (10), 3138−3143.
(14) Bonnett, R. Photosensitizers of the Porphyrin and Phthalocyanine Series for Photodynamic Therapy. *Chem. Soc. Rev.* **1995**, *24* (1), 19−33.
(15) Zhang, X.-F.; Xu, H.-J. Influence of Halogenation and Aggregation on Photosensitizing Properties of Zinc Phthalocyanine (ZnPC). *J. Chem. Soc., Faraday Trans.* **1993**, *89* (18), 3347−3351.
(16) Kuznetsova, N. A.; Gretsova, N. S.; Derkacheva, V. M.; Kaliya, O. L.; Lukyanets, E. A. Sulfonated Phthalocyanines: Aggregation and Singlet Oxygen Quantum Yield in Aqueous Solutions. *J. Porphyrins Phthalocyanines* **2003**, *7* (3), 147−154.
(17) Colussi, V. A.; Feyes, D. K.; Mulvihill, J. W.; Li, Y. S.; Kenney, M. E.; Elmets, C. A.; Oleinick, N. L.; Mukhtar, H. Phthalocyanine 4 (Pc 4) Photodynamic Therapy of Human OVCAR-3 Tumor Xenografts. *Photochem. Photobiol.* **1999**, *69* (2), 236−241.
(18) Doane, T. L.; Chuang, C. H.; Chomas, A.; Burda, C. Photophysics of Silicon Phthalocyanines in Aqueous Media. *ChemPhysChem* **2013**, *14* (2), 321−330.
(19) Ganesh, V. A.; Raut, H. K.; Nair, A. S.; Ramakrishna, S. A Review on Self-Cleaning Coatings. *J. Mater. Chem.* **2011**, *21* (41), 16304−16322.
(20) Yadanaparthi, S. K.; Graybill, D.; von Wandruszka, R. Adsorbents for the Removal of Arsenic, Cadmium, and Lead from Contaminated Waters. *J. Hazard. Mater.* **2009**, *171*, 1−15.
(21) Shi, J.; Bian, W.; Yin, X. Organic Contaminants Removal by the Technique of Pulsed High-Voltage Discharge in Water. *J. Hazard. Mater.* **2009**, *171*, 924−931.
(22) Martínez-Huitle, C. A.; Brillas, E. Electrochemical Alternatives for Drinking Water Disinfection. *Angew. Chem., Int. Ed.* **2008**, *47*, 1998−2005.
(23) Martínez-Huitle, C. A.; Brillas, E. Elektrochemische Alternativen für die Trinkwasserdesinfektion. *Angew. Chem.* **2008**, *120*, 2024−2032.
(24) Litter, M. I.; Quici, N. Photochemical Advanced Oxidation Processes for Water and Wastewater Treatment. *Recent Pat. Eng.* **2010**, *4* (3), 217−241.
(25) Legrini, O. E.; Oliveros, E.; Braun, A. M. Photochemical Processes for Water Treatment. *Chem. Rev.* **1993**, *93* (2), 671−698.
(26) Zharov, V. P.; Mercer, K. E.; Galitovskaya, E. N.; Smeltzer, M. S. Photothermal Nanotherapeutics and Nanodiagnostics for Selective Killing of Bacteria Targeted with Gold Nanoparticles. *Biophys. J.* **2006**, *90* (2), 619−627.
(27) Radovic-Moreno, A. F.; Lu, T. K.; Puscasu, V. A.; Yoon, C. J.; Langer, R.; Farokhzad, O. C. Surface Charge-Switching Polymeric Nanoparticles for Bacterial Cell Wall-Targeted Delivery of Antibiotics. *ACS Nano* **2012**, *6* (5), 4279−4287.
(28) Lin, C.-C.; Yeh, Y.-C.; Yang, C.-Y.; Chen, C.-L.; Chen, G.-F.; Chen, C.-C.; Wu, Y.-C. Selective Binding of Mannose-Encapsulated Gold Nanoparticles to Type 1 Pili in Escherichia coli. *J. Am. Chem. Soc.* **2002**, *124* (14), 3508−3509.
(29) El-Boubbou, K.; Gruden, C.; Huang, X. Magnetic Glyconanoparticles: A Unique Tool for Rapid Pathogen Detection, Decontamination, and Strain Differentiation. *J. Am. Chem. Soc.* **2007**, *129* (44), 13392−13393.
(30) Strassert, C. A.; Otter, M.; Albuquerque, R. Q.; Höne, A.; Vida, Y.; Maier, B.; De Cola, L. Photoactive Hybrid Nanomaterial for Targeting, Labeling, and Killing Antibiotic-Resistant Bacteria. *Angew. Chem., Int. Ed.* **2009**, *48* (42), 7928−7931.
(31) Strassert, C. A.; Otter, M.; Albuquerque, R. Q.; Höne, A.; Vida, Y.; Maier, B.; De Cola, L. Photoaktive hybride Nanomaterialien für gezieltes Anbinden, Markieren und Töten von Antibiotika-resistenten Bakterien. *Angew. Chem.* **2009**, *121* (42), 8070−8073.
(32) Reddy, P. M.; Chang, K.-C.; Liu, Z.-J.; Chen, C.-T.; Ho, Y-.P. Functionalized Magnetic Iron Oxide (Fe_3O_4) Nanoparticles for Capturing Gram-Positive and Gram-Negative Bacteria. *J. Biomed. Nanotechnol.* **2014**, *10* (8), 1429−1439.
(33) Grüner, M.; Siozios, V.; Hagenhoff, B.; Breitenstein, D.; Strassert, C. A. Structural and Photosensitizing Features of Phthalocyanine—Zeolite Hybrid Nanomaterials. *Photochem. Photobiol.* **2013**, *89* (6), 1406−1412.
(34) Lezhnina, M. M.; Grewe, T.; Stoehr, H.; Kynast, U. Laponite Blue: Dissolving the Insoluble. *Angew. Chem., Int. Ed.* **2012**, *51* (42), 10652−10655.
(35) Lezhnina, M. M.; Grewe, T.; Stoehr, H.; Kynast, U. Laponite-Blau: eine Lösung für Unlösliches. *Angew. Chem.* **2012**, *124* (42), 10805−10809.
(36) Choy, J.-H.; Choi, S.-J.; Oh, J.-M.; Park, T. Clay Minerals and Layered Double Hydroxides for Novel Biological Applications. *Appl. Clay Sci.* **2007**, *36* (1−3), 122−132.
(37) Viseras, C.; Aguzzi, C.; Cerezo, P.; Lopez-Galindo, A. Uses of Clay Minerals in Semisolid Health Care and Therapeutic Products. *Appl. Clay Sci.* **2007**, *36* (1−3), 37−50.
(38) Carreto, M. I.; Gomes, C. S. F.; Tateo, F. Clays, Drugs, and Human Health. In *Developments in Clay Science*; Bergaya, F., Lagaly, G., Eds.; Elsevier: Oxford, 2013; pp 711, Chapter 5.5.
(39) Ghardiri, M.; Chrzanowski, W.; Rohanizadeh, R. Antibiotic Eluting Clay Mineral (Laponite) for Wound Healing Application: an in Vitro Study. *J. Mater. Sci.: Mater. Med.* **2014**, *25* (11), 2513−2526.
(40) Viseras, C.; Cerezo, P.; Sanchez, R.; Salcedo, I.; Aguzzi, C. Current Challenges in Clay Minerals for Drug Delivery. *Appl. Clay Sci.* **2010**, *48* (3), 291−295.

DOI: 10.1021/acsami.5b06742
ACS Appl. Mater. Interfaces 2015, 7, 20965−20971

(41) Mortimer, G. M.; Butcher, N. J.; Musumeci, A. W.; Deng, Z. J.; Martin, D. J.; Minchin, R. F. Cryptic Epitopes of Albumin Determine Mononuclear Phagocyte System Clearance of Nanomaterials. *ACS Nano* **2014**, *8* (4), 3357−3366.
(42) Li, K.; Wang, S.; Wen, S.; Tang, Y.; Li, J.; Shi, X.; Zhao, Q. Enhanced In Vivo Antitumor Efficacy of Doxorubicin Encapsulated within Laponite Nanodisks. *ACS Appl. Mater. Interfaces* **2014**, *6* (15), 12328−12334.
(43) Wu, Y.; Guo, R.; Wen, S.; Shen, M.; Zhu, M.; Wang, J.; Shi, X. Folic Acid-modified Laponite Nanodisks for Targeted Anticancer Drug Delivery. *J. Mater. Chem. B* **2014**, *2*, 7410−7418.
(44) Wang, S.; Wu, Y.; Guo, R.; Huang, Y.; Wen, S.; Shen, M.; Wang, J.; Shi, X. Laponite Nanodiscs as an Efficient Platform for Doxorubicin Delivery to Cancer Cells. *Langmuir* **2013**, *29* (16), 5030−5036.
(45) Gonçalves, M.; Figueira, P.; Maciel, D.; Rodrigues, J.; Shi, X.; Tomás, H.; Li, Y. Antitumor Efficacy of Doxorubicin-Loaded Laponite/Alginate Hybrid Hydrogels. *Macromol. Biosci.* **2014**, *14* (1), 110−120.
(46) Strassert, C. A.; Rodriguez, M. E.; Dicelio, L. E.; Awruch, J. A Synthetic Approach Towards Novel Octa-Substituted Zinc(II) Phthalocyanines with Different Solubility and Photophysical Properties. *J. Porphyrins Phthalocyanines* **2005**, *9* (5), 361−367.
(47) Doane, T.; Chomas, A.; Srinivasan, S.; Burda, C. Observation and Photophysical Characterization of Silicon Phthalocyanine J-Aggregate Dimers in Aqueous Solutions. *Chem. - Eur. J.* **2014**, *20* (26), 8030−8039.
(48) Rodríguez, H. B.; San Román, E. Effect of Concentration on the Photophysics of Dyes in Light-Scattering Materials. *Photochem. Photobiol.* **2013**, *89* (6), 1273−1282.
(49) Skovsen, E.; Snyder, J. W.; Lambert, J. D. C.; Ogilby, P. R. Lifetime and Diffusion of Singlet Oxygen in a Cell. *J. Phys. Chem. B* **2005**, *109* (18), 8570−8573.

DOI: 10.1021/acsami.5b06742
ACS Appl. Mater. Interfaces 2015, 7, 20965−20971